Modeling PCDH19 Related Epilepsy in Human Pluripotent Stem Cell Derived Brain Organoids

Roksolana Sudyk

Sponsor: Jack Parent, M.D.
Co-Sponsor: Richard Hume, Ph.D.
Reader: Laura Olsen, Ph.D.

Date of Submission: March 22, 2021

A thesis submitted in partial fulfillment of the Degree of Bachelor of Science in Neuroscience with Honors

PCDH19 Related Epilepsy (PRE) is an X-linked disorder with a unique inheritance pattern, in which heterozygous females and mosaic males are affected, but hemizygous males (carrier males) are unaffected. PRE is caused by the random X-inactivation of the *PCDH19* gene, which causes the mosaic expression of the PCDH19 protein and the co-existence of PCDH19-positive cells and PCDH19-mutant cells in heterozygous females and mosaic males. The co-existence of PCDH19-positive cells and PCDH19-mutant cells causes altered cell-to-cell communication and abnormal cell sorting, which may alter neuronal circuitry during the development of the brain and cause neuronal hyperexcitability and seizures. Recent research employing mouse models have made significant progress in our understanding of the mechanism of PRE. However, given the differences in the development of the brain between mice and humans, mouse models alone are insufficient for understanding the role of *PCDH19* mosaic expression in PRE. Therefore, in our research, we differentiated human pluripotent stem cells into single-rosette organoids of the cerebral cortex and ganglionic eminences to understand the role of *PCDH19* mosaic expression during the development of the brain, and thus, the neurodevelopmental effects of PRE. In our research, we found that mixed wildtype-wildtype "healthy" organoids and mixed *PCDH19* knockout- knockout "carrier" organoids showed the expected patterns of cell mixing, whereas mixed wildtype-*PCDH19* knockout "PRE" organoids showed abnormal cell sorting, as well as abnormal cytoarchitecture. Our findings demonstrate that human pluripotent stem cell and organoid models can provide insights into the phenotypes and mechanisms of PRE. Broadly, a similar organoid system may be employed to study other neurodevelopmental disorders.

TABLE OF CONTENTS

SCIENTIFIC ACKNOWLEDGEMENTS

The experiments in this thesis were completed in close collaboration with Wei Niu, Ph.D., a research assistant professor, and Sandra Mojica-Perez, a research lab specialist in Dr. Parent's laboratory, and they have granted permission to include some data that they collected and analyzed in this thesis. The person who conducted each experiment in this thesis is indicated in this table:

Figure	Person Who Conducted the Experiment
1	A: Sandra Mojica-Perez collected and analyzed the data on the cortical organoids; Wei Niu and I collected and analyzed the data on the ventral organoids B: Wei Niu and I prepared the sample; I performed immunocytochemistry, imaging, and data analysis
2	Sandra Mojica-Perez prepared the sample and performed imaging on the data; I performed data analysis
3	Sandra Mojica-Perez and I prepared the sample; I performed immunocytochemistry, imaging, and data analysis
4	Sandra Mojica-Perez and I prepared the sample; I performed immunocytochemistry, imaging, and data analysis; Wei Niu assisted with statistical analysis
5	Wei Niu and I prepared the sample; I performed immunocytochemistry, imaging, and data analysis; Wei Niu assisted with statistical analysis
6	Wei Niu and I prepared the sample; I performed immunocytochemistry, imaging, and data analysis; Wei Niu assisted with statistical analysis
7	Wei Niu and I prepared the sample; I performed immunocytochemistry, imaging, and data analysis; Wei Niu assisted with statistical analysis
8	Wei Niu and I prepared the sample; I performed immunocytochemistry, imaging, and data analysis; Wei Niu assisted with statistical analysis
9	Wei Niu prepared the sample and performed imaging on the data; I performed data analysis
10	Wei Niu and I prepared the sample; I performed immunocytochemistry, imaging, and data analysis

PERSONAL ACKNOWLEDGEMENTS

I would like to thank Dr. Jack Parent for the opportunity to perform research in his laboratory, as well as Dr. Elmira Jalilian, Dr. Wei Niu, and Ms. Sandra Mojica-Perez for their mentorship over the past three years. I would also like to thank Dr. Andrew Tidball, who is a research investigator in Dr. Parent's laboratory, for his technical support, as he developed the single-rosette organoid model. I would also like to thank my parents, Vasyl and Lisa Sudyk, as well as my sister, Christina Sudyk, for their encouragement in my writing this thesis.

INTRODUCTION

PCDH19 Related Epilepsy (PRE) has been referred to as "Epilepsy and Mental Retardation Limited to Females" and "PCDH19 Girls Clustering Epilepsy." In 1971, Juberg and Hellman coined the term "Epilepsy and Mental Retardation Limited to Females" (EFMR) to describe an early onset epileptic disorder in females. In 2008, researchers identified *PCDH19* variations as the genetic cause of EFMR (Dibbens et al., 2008). Around this time, researchers coined the term "PCDH19 Girls Clustering Epilepsy" (PCDH19-GCE) to incorporate the genetic component of the epileptic disorder in females (Dibbens et al., 2008). In 2009, researchers identified *PCDH19* mutations and PCDH19-GCE symptoms in mosaic males (Depienne et al., 2009; Terracciano et al., 2016; Thiffault et al., 2016). Recently, researchers coined the term PRE to incorporate the male experience of the epileptic disorder (Terracciano et al., 2016).

PRE is defined as an early onset seizure disorder with a varied neuropsychiatric profile, including intellectual disability, and autistic, attention-deficit, hyperactive, or aggressive features (Juberg and Hellman, 1971; Scheffer et al., 2008). It is the second most common cause of monogenic epilepsy (Pederick et al., 2018). PRE patients have an average age of seizure onset of 11.9 months, which is precipitated and accompanied by a fever in 80% of the cases (Kolc et al., 2019). The seizures may begin as focal seizures that become generalized tonic-clonic seizures, or the seizures may have generalized onset. In adolescence, the seizures may reduce in frequency or intensity. However, in adolescence, neuropsychiatric dysfunctions may escalate (Kolc et al., 2019). Of the reported PRE cases, 59.1% show comorbidities – 19.7% show comorbidities with Autism Spectrum Disorder, 11.7% with Attention-Deficit-Hyperactivity Disorder, 6.1% with additional behavioral disorders, and 21.6% show several comorbidities (Kolc et al., 2019). PRE is an X-linked disorder with a unique inheritance pattern. Of the reported cases, 50.2% are de novo whereas 49.8% are familial (Kolc et al., 2019). Of the reported familial cases, 81.3% are paternally inherited (Kolc et al., 2019). As an X-linked disorder, it would be expected that it would be more severe in hemizygous males; however, heterozygous females and mosaic males are affected, while hemizygous males are unaffected (Pederick et al., 2018).

PRE is caused by mutations in the *PCDH19* gene on the X chromosome, which is expressed in the brain, particularly in the cerebral cortex, hippocampus, and amygdala (Kim et al., 2007). The *PCDH19* gene is composed of six exons: exon one encodes the extracellular domain, the transmembrane domain, and part of the intracellular domain of the PCDH19 protein;

exons two through six encode the intracellular domain of the PCDH19 protein. The *PCDH19* gene encodes a 1148 amino acid PCDH19 protein (Kolc et al., 2019). Approximately 150 mutations, including whole gene deletions, partial gene deletions, missense mutations, frameshift mutations, and nonsense mutations, have been identified in the *PCDH19* gene, causing disease (Gerosa et al., 2019). PRE mutations are thus considered to be loss-of-function mutations, and most occur in the extracellular domain. Of the reported PRE cases, 86.7% are extracellular domain mutations, which are thought to impair PCDH19-mediated cell-to-cell interactions (Kolc et al., 2019). The extracellular domain is composed of six repeats that are involved in cell-to-cell interactions. According to the forearm handshake model, protocadherin direct cell-to-cell interactions involve an antiparallel interaction between two protocadherins through a trans interface, forming a protocadherin dimer. Additionally, protocadherin indirect cell-to-cell interactions involve a parallel interaction between a protocadherin and n-cadherin through a cis interface, forming a protocadherin-n-cadherin dimer (Gerosa et al., 2019).

The unique inheritance pattern of PRE may be explained by the cellular interference model, which theorizes that random X-inactivation of the *PCDH19* gene causes the co-existence of PCDH19-positive and PCDH19-negative cells, impairing cell-to-cell interactions. PCDH19-positive and PCDH19-negative cells have repulsive chemoaffinity labels; therefore, PCDH19-postive and PCDH19-negative cells show self-avoidance and segregation (Dibbens et al., 2008). Pederick et al. (2018) employed *in vitro* studies, as well as *in vivo* studies via a mouse model, to mimic mosaic PCDH19 activity in PRE. In order to understand PCDH19 activity *in vitro*, the researchers expressed wildtype *PCDH19* and variant *PCDH19.N340S* in K562 cells, which lack endogenous protocadherins. The researchers found that wildtype *PCDH19* K562 cells underwent cell mixing with other wildtype *PCDH19* K562 cells, and variant *PCDH19.N340S* K562 cells underwent cell mixing with other variant *PCDH19.N340S* K562 cells (Pederick et al., 2018). However, the researchers found that wildtype *PCDH19* K562 cells underwent cell sorting with variant *PCDH19.N340S* K562 cells, with wildtype cells interacting with wildtype cells only and variant cells interacting with variant cells only (Pederick et al., 2018). Moreover, in order to understand PCDH19 activity *in vivo*, the researchers created a female *Pcdh19* heterozygous knockout mouse model expressing the wildtype *Pcdh19* allele and the variant *Pcdh19.N340S* allele, labeling the wildtype *Pcdh19* allele only. The researchers found segregation of PCDH19-positive cells from PCDH19-negative cells, with PCDH19-positive cells interacting with

PCDH19-positive cells only and PCDH19-negative cells interacting with PCDH19-negative cells only. According to immunostaining analyses, the segregation of PCDH19-positive cells from PCDH19-negative cells begins between embryonic day 9.5-10.5 and continues into the postnatal period (Pederick et al., 2018). Additionally, the segregation of PCDH19-positive cells from PCDH19-negative cells spans from the ventricular zone to the cortical plate (Pederick et al., 2018). Moreover, the PCDH19 protein is expressed at the cellular interface of PCDH19-positive cells and other PCDH19-positive cells but is absent at the cellular interface between PCDH19-postive cells and PCDH19-negative cells (Pederick et al., 2018). Pederick et al.'s (2018) results suggest that homogeneous expression of *PCDH19/Pcdh19* causes self-attraction due to attractive chemoaffinity labels, whereas heterogeneous expression of *PCDH19*/*Pcdh19* causes self-avoidance due to repulsive chemoaffinity labels.

Although mouse models have been instrumental in the understanding of the cellular interference model of PRE, mouse models alone are insufficient in the understanding of the cellular mechanism of PRE, as it relates to humans. During the development of the cerebral cortex, the proliferation of cells creates wedges of cell-dense and cell-sparse areas, influencing cerebral cortical folding. In the case of PRE, PCDH19 self-avoidance and segregation may cause irregular proliferation of cells, which may create irregular wedges of cell-dense and cell-sparse areas, influencing cerebral cortical folding. In addition, in the case of PRE, PCDH19 self-avoidance and segregation may cause irregular synaptogenesis across cerebral cortical areas, perturbing cerebral cortical boundaries (Pederick et al., 2018). However, the development of the cerebral cortex in mice considerably differs from that in humans.

In humans, the cerebral cortex is organized into the ventricular zone, the subventricular zone, and the cortical plate, which is organized into six layers or lamina (Soriano and Del Rio, 2005; Stoykova et al., 2003). The ventricular zone is composed of apical radial glial cells (Hansen et al., 2010). Apical radial glial cells have apical processes that extend to the cortical ventricle and basal processes that extend to the cortical pia (Hansen et al., 2010). Apical radial glial cells undergo symmetrical and asymmetrical divisions. Symmetrical divisions, caused by vertical divisions along a vertical cleavage plane, give rise to two identical cells – two apical radial glial cells. Asymmetrical divisions, caused by horizontal divisions along a horizontal cleavage plane, give rise to two unidentical cells – one apical radial glial cell and either one basal radial glial cell or one intermediate progenitor cell (Hansen et al., 2010). Whereas the apical

radial glial cells remain in the ventricular zone, the basal radial glial cells and intermediate progenitor cells migrate to the subventricular zone, utilizing apical radial glial basal processes as scaffolds (Hansen et al., 2010). The subventricular zone is composed of basal radial glial cells and intermediate progenitor cells (Hansen et al., 2010). Similar to apical radial glial cells, basal radial glial cells have basal processes that extend to the cortical pia (Hansen et al., 2010). Moreover, similar to apical radial glial cells, basal radial glial cells undergo symmetrical and asymmetrical divisions. Symmetrical divisions give rise to two basal radial glial cells. Asymmetrical divisions give rise to one basal radial glial cell and one intermediate progenitor cell (Hansen et al., 2010). The basal radial glial cells and intermediate progenitor cells remain in the subventricular zone (Hansen et al., 2010). The intermediate progenitor cells give rise to neurons (Hansen et al., 2010). The neurons migrate to the cortical plate, utilizing apical radial glial basal processes and basal radial glial basal processes as scaffolds (Hansen et al., 2010). The intermediate progenitor cells give rise to different neurons at different times. First, the intermediate progenitor cells give rise to cajal-retzius cells. The cajal-retzius cells migrate to the outside aspect, layer one, of the cortical plate. There, the cajal-retzius cells express and secrete REELIN, which regulates the migration of the remaining neurons into the remaining five lamina of the cortical plate (Soriano and Del Rio, 2005; Stoykova et al., 2003). Neurons born at earlier times migrate to the deeper lamina of the cortical plate, such as layers six, five, and four. Neurons born at later times migrate to the shallower lamina of the cortical plate, such as layers three and two (Soriano and Del Rio, 2005; Stoykova et al., 2003).

The cerebral cortex is composed of excitatory glutamatergic neurons and inhibitory GABAergic neurons (Xiang et al., 2017). The excitatory glutamatergic neurons arise from the pallium, the dorsal area of the telencephalic anlage that gives rise to the cerebral cortex, cortical hem, and choroid plexus, whereas the inhibitory GABAergic neurons arise from the ganglionic eminences in the subpallium, the ventral area of the telencephalic anlage that gives rise to the basal ganglion, as well as cortical and olfactory bulb interneurons (Xiang et al., 2017). During the development of the cerebral cortex, GABAergic interneurons migrate to the cerebral cortex from the ganglionic eminences, utilizing tangential pathways (Liu et al., 2013). In the cerebral cortex, ganglionic eminence progenitors differentiate into GABAergic interneurons, synapsing onto glutamatergic neurons or other interneurons (Liu et al., 2013). Thus, GABAergic interneurons are able to modulate neuronal network activity and neuronal plasticity.

In contrast to the development of the cerebral cortex in humans, the development of the cerebral cortex in mice is more simplistic. The human cerebral cortex is larger than the mouse cerebral cortex (Herculano-Houzel, 2009). The human cerebral cortex contains a more prominent subventricular zone, diverging into an inner subventricular zone and an outer subventricular zone. In addition, the human cerebral cortex contains more basal radial glial cells, undergoing more symmetrical and asymmetrical divisions, giving rise to more basal radial glial cells and intermediate progenitor cells. Thus, the human cerebral cortex generates a greater proliferative output (Zecevic et al., 2005). Given the distinctions in development of the cerebral cortex in humans from that in mice, the mouse model is likely insufficient to mimic the development of the cerebral cortex in PRE. This limitation provides an impetus to implement human pluripotent stem cell (either human induced pluripotent stem cell or human embryonic pluripotent stem cell) models to mimic the development of the cerebral cortex in PRE.

Human induced pluripotent stem cells are able to differentiate and organize into cerebral cortical-like and ganglionic eminence-like structures. Okita et al. (2007) employed somatic cells, fibroblasts, to create induced pluripotent stem cells through the transduction of the transcription factors OCT3/4, SOX2, KLF4, and C-MYC. C-MYC is a proto-onco-gene that triggers the reprogramming into induced pluripotent stem cells. OCT3/4, SOX2, and KLF4 are pluripotent genes that maintain the transformation into induced pluripotent stem cells (Okita et al., 2007). As soon as the somatic cells are reprogrammed into induced pluripotent stem cells, the transcription factors are not required for the maintenance of the induced pluripotent stem cells (Okita et al., 2007). At this time, the human induced pluripotent stem cells are able to differentiate and organize into embryoids, three-dimensional structures that mimic the human embryo.

In order to model the human embryonic brain in two dimensions, Liu et al. (2013) described a method to generate both cerebral cortical neurons and ganglionic eminence interneurons. In order to generate cerebral cortical neurons, Liu et al. (2013) introduced FGF2 to induced pluripotent stem cells to induce glutamatergic neuronal stem cell fate. Following the introduction of FGF2, the glutamatergic neuronal stem cells express FOXG1, a telencephalic marker, as well as PAX6, SOX1, SOX2, NCAD and NESTIN, glutamatergic neuronal stem cell markers (Liu et al., 2013). In order to generate ganglionic eminence interneurons, Liu et al. (2013) introduced FGF2, as well as Sonic Hedgehog, to induced pluripotent stem cells to induce GABAergic interneuronal stem cell fate. Following the introduction of FGF2 and Sonic

Hedgehog, the GABAergic interneuronal stem cells express FOXG1, a telencephalic marker, NKX2.1, a ganglionic eminence marker, as well as SST and GABA, GABAergic interneuronal markers (Liu et al., 2013). Similarly, in order to model the human embryonic brain in three dimensions, Xiang et al. (2017) described a method to generate cerebral cortical organoids through directed differentiation, whereas Birey et al. (2017) described a method to generate ganglionic eminence organoids through directed differentiation. In order to generate cerebral cortical organoids, Xiang et al. (2017) introduced Dual SMAD inhibition and Canonical WNT inhibition to induced pluripotent stem cells to induce glutamatergic neuronal stem cell fate. In order to generate ganglionic eminence organoids, Birey et al. (2017), introduced Dual SMAD inhibition, as well as IWP2 and SAG, to induced pluripotent stem cells to induce GABAergic interneuronal stem cell fate. IWP2 and SAG are modulators of the WNT and Sonic Hedgehog pathways, respectively, thus additional inducers of GABAergic interneural fate. Additionally, in their article, Watanabe et al. (2017) outlined additional methods to increase the efficacy of cerebral cortical organoid generation, and Birey et al. (2017) outlined additional methods to increase the efficacy of ganglionic eminence organoid generation. In order to increase the efficacy of cerebral cortical organoid generation, Watanabe et al. (2017) suggest the addition of LIF to increase the amount of glutamatergic neuronal stem cells, as well as to enlarge the subventricular zone. In order to increase the efficacy of ganglionic eminence organoid generation, Birey et al. (2017) suggest the omission of NGF to increase the amount of GABAergic interneuronal stem cells. It is important to note that the ganglionic eminences are able to give rise to GABAergic interneuronal progenitors and cholinergic neuronal progenitors. NGF is an inducer of cholinergic neuronal stem cell fate. Thus, through the omission of NGF, Birey et al. (2017) are able to generate ganglionic eminence organoids with a purity of 90%. A number of methods have been utilized to successfully generate cerebral cortical organoids and ganglionic eminence organoids. Nevertheless, regardless of the method of organoid generation, the cerebral cortical organoids and ganglionic eminence organoids are able to mimic the development of the human cerebral cortex.

Cerebral cortical organoids are able to mimic the development of the human cerebral cortex *in vivo*. Cerebral cortical organoids express FOXG1, a telencephalic marker, and PAX6, a glutamatergic neuronal stem cell marker (Xiang et al., 2017). Cerebral cortical organoids express SOX2, an apical radial glial cell marker, FAM107A, a basal radial glial cell marker, TBR2, an

intermediate progenitor cell marker, CTIP2, a cortical layer V marker, SATB2, a cortical layer II marker, and REELIN, a cortical layer I marker (Xiang et al., 2017). The expression of ventricular zone, subventricular zone, and cortical plate markers suggests the formation of a ventricular zone, subventricular zone, and cortical plate, with up to six lamina, in the cerebral cortical organoids. Likewise, cerebral cortical organoids express NCAD, an apical adherin marker, and pH3, a dividing cell marker, in the apical membrane, as well as TuJ1, a neuronal marker, and GFAP, an astroglial marker, in the basal membrane (Xiang et al., 2017). The co-expression of NCAD and pH3 in the apical membrane indicates the proliferation of apical radial glial cells in the apical membrane. According to Xiang et al. (2017), 58% of apical radial glial cells undergo vertical division to give rise to two apical radial glial cells, whereas 42% of apical radial glial cells undergo horizontal division to give rise to one apical radial glial cell and either one basal radial glial cell or one intermediate progenitor cell. The co-expression of TuJ1 and GFAP in the basal membrane indicates the migration and aggregation of neuronal and astroglial cells in the basal membrane. Thus, the expression of apical membrane and basal membrane markers indicates a radial organization in the cerebral cortical organoids. In addition, according to patch-clamp recordings of cerebral cortical organoids, cerebral cortical neurons exhibit action potentials that are tetrodotoxin sensitive, as well as significant sodium and potassium currents (Watanabe et al., 2017). Likewise, according to patch-clamp recordings of cerebral cortical organoids, cerebral cortical neurons show similar membrane potentials, membrane resistances, peak sodium currents, and peak potassium currents as cerebral cortical neurons *in vivo* (Watanabe et al., 2017). Furthermore, according to transcriptomic analyses of cerebral cortical organoids, cerebral cortical neurons express CAMKII, SYNAPSIN, VGLUT1, and SYNAPTOTAGMIN1, which is similar to cerebral cortical neurons *in vivo* (Watanabe et al., 2017). The patch-clamp recording and transcriptomic analysis results represent the structural and functional features of neurons, including calcium signaling and synaptogenesis, suggesting that cerebral cortical organoids contain functional neurons. Moreover, according to gene co-expression network analyses of cerebral cortical organoids, at least 14 out of 28 cerebral cortical modules were conserved in cerebral cortical organoids, including RNA processing, DNA repair, ubiquitin proteolysis, neural progenitor mitosis, neurogenesis, gliogenesis, axon guidance, synaptogenesis, and synaptic transmission (Watanabe et al., 2017). The gene co-expression network analysis results represent the correlation between cellular and biochemical processes in

the cerebral cortex *in vivo* and the cerebral cortical organoids *in vitro*, suggesting that cerebral cortical organoids preserve cellular and biochemical processes related to the development and differentiation of neurons in the cerebral cortex *in vivo*. At last, according to transition mapping analyses of cerebral cortical organoids, the transition from 5-week cerebral cortical organoids to 14-week cerebral cortical organoids mimics the transition from first trimester embryonic cerebral cortical development to mid-fetal cerebral cortical development *in vivo* (Watanabe et al., 2017). The transition mapping analysis results represent the correlation between the development in the cerebral cortex *in vivo* and the cerebral cortical organoids *in vitro*, suggesting that cerebral cortical organoids mimic the development of the cerebral cortex *in vivo*. These findings suggest that cerebral cortical organoids are useful *in vitro* models of the development of the human cerebral cortex.

Ganglionic eminence organoids are able to mimic the development of the human ganglionic eminences *in vivo*. Ganglionic eminence organoids express FOXG1, a telencephalic marker, and NKX2.1, a ganglionic eminence marker. Ganglionic eminence organoids express DLX2 and ALSC1, GABAergic interneuronal stem cell markers. Likewise, ganglionic eminence organoids express GAD67, a GABA-synthesizing enzyme marker, as well as GABA, SST, CR, CB, and PV, GABAergic interneuronal markers (Birey et al., 2017). In addition, according to patch-clamp recordings of ganglionic eminence organoids, 75% of ganglionic eminence interneurons show action potentials and 60% show spontaneous inhibitory postsynaptic currents that are allopregnanolone and gabazine sensitive (Birey et al., 2017). Furthermore, according to microarray analyses of ganglionic eminence organoids, ganglionic eminence interneurons express SYN1 and VGAT, which is similar to ganglionic eminence interneurons *in vivo* (Birey et al., 2017). The patch-clamp recording and microarray analysis results represent the structural and functional features of interneurons, including calcium signaling and synaptogenesis, suggesting that ganglionic eminence organoids contain functional interneurons. These findings suggest that ganglionic eminence organoids are models *in vitro* models of the development of the human ganglionic eminences and cortical interneurons.

The fusion of cerebral cortical organoids and ganglionic eminence organoids allows for the migration of GABAergic interneurons from the ganglionic eminence organoids to the cerebral cortical organoids, as well as the integration of GABAergic interneurons with glutamatergic networks in the cerebral cortex, and thus generates a useful *in vitro* model of the

human cerebral cortex. In their article, Birey et al. (2017) outlined a method to fuse cerebral cortical organoids and ganglionic eminence organoids spontaneously in an eppendorf tube. The cerebral cortical organoids and ganglionic eminence organoids fused within three days. Birey et al. (2017) employed viral labelling of ganglionic eminence GABAergic interneurons in order to track the migration, maturation, and integration of the GABAergic interneurons into the cerebral cortex. In their migration from the ganglionic eminences to the cerebral cortex, the GABAergic interneurons undergo unidirectional saltatory movement involving the extension of the GABAergic interneuonal leading process, the swelling of the GABAergic interneuronal soma, and, at last, the GABAergic interneuronal nuclear translocation, which is similar to the migration of GABAergic interneurons in the cerebral cortex *in vivo* (Birey et al., 2017). After 14 days, the GABAergic interneurons express DLX1, DLX2, DLX5, and DLX6, ganglionic eminence markers, as well as GAD1, GAD2, VGAT, and CEL4, GABAergic interneuronal markers (Birey et al., 2017). After 28 days, the GABAergic interneurons decrease expression of PDX3, a ganglionic eminence marker. Additionally, after 28 days, the GABAergic interneurons increase expression of SOX1, ERBB4, NNAT, MALAT1, and NXPH1, interneuronal migration markers (Birey et al., 2017). Such changes in expression indicate that GABAergic interneurons are successfully migrating and integrating into the cerebral cortex. Furthermore, after 28 days, the GABAergic interneurons increase branching. Additionally, after 28 days, the GABAergic interneurons show more frequent action potentials, as well as excitatory and inhibitory synaptic inputs and outputs (Birey et al., 2017). Such changes in structure and function indicate that GABAergic interneurons are successfully synapsing with glutamatergic neurons in the cerebral cortex. Therefore, the fusion of cerebral cortical organoids and ganglionic eminence organoids is able to mimic the development of the human cerebral cortex.

There are challenges in the creation of organoids that mimic the development of the human cerebral cortex. The cerebral cortex forms from a single neuroepithelial unit, which is the center of morphogenesis. The center of morphogenesis localizes neuronal stem cells in the apical membrane, so that neurons migrate to the basal membrane, where they expand the cerebral cortex. The breakdown of the center of morphogenesis causes severe congenital disorders *in vivo* (Knight et al., 2018). However, organoids tend to form several neuroepithelial units, which are separate centers of morphogenesis (Knight et al., 2018). In order to create organoids that mimic

the development of the human cerebral cortex with greater reliability, it would be beneficial to generate single rosette organoids.

In their article, Knight et al. (2018) outlined a method to generate single rosette organoids. Organoids undergo pre-polarization, polarization, and rosette formation phases. In the pre-polarization phase, organoid pluripotent stem cells undergo neural induction. At the end of the phase, organoids express PAX6, a neuronal stem cell marker. In the polarization phase, organoid neuronal stem cells migrate to the apical membrane. At the end of the phase, organoids express NCAD and ZO-1, apical neuronal stem cell markers. At last, in the rosette formation stage, organoid neuronal stem cells connect to create a circle at the apical membrane. At the end of the phase, organoids increase expression of NCAD and ZO-1, which are adherin and junction proteins, respectively (Knight et al., 2018). Knight et al. (2018) restricted organoids' size and shape by isolation on two-dimensional micropatterned wells of specific sizes and shapes in order to favor the formation of single rosette organoids. Following the isolation of cerebral cortical organoids on circular, as compared to square, triangle, and oblong, micropatterns of 200-250 micrometers, as compared to 100 micrometers, 150 micrometers, 180 micrometers, 300 micrometers, and 400 micrometers, the cerebral cortical organoids form single rosettes with 80-85% efficiently. Otherwise, following the isolation of ganglionic eminence organoids on circular micropatterns of 150 micrometers, the ganglionic eminence organoids form single rosettes with 73.5% efficiency (Knight et al., 2018). Additionally, Knight et al. (2018) found a direct relationship between organoids' capacity for proliferation and organoids' ability for formation of single rosettes. Conversely, Knight et al. (2018) found an inverse relationship between organoids' surface area and organoids' ability for formation of single rosettes. Thus, younger organoids are able to form single rosettes with the greatest efficiency. Following the emancipation of organoids from the two-dimensional micropatterned wells of specific sizes and shapes, the organoids maintain a single rosette. Indeed, the organoids expanded and differentiated radially (Knight et al., 2018). Single rosette organoids are able to better model the development of the nervous system.

Organoid models are able to mimic the development and organization of the cerebral cortex to model neurodevelopmental disorders. Birey et al. (2017) employed an organoid model to model the development of Timothy Syndrome in the developing cerebral cortex. Timothy Syndrome is a neurodevelopmental disease characterized by autism spectrum disorder and

epilepsy. Timothy Syndrome is caused by a mutation in l-type calcium channels, which modulate GABAergic interneuron migration in the developing cerebral cortex (Birey et al., 2017). Birey et al. (2017) generated typical cerebral cortical-ganglionic eminence fused organoids, as well as atypical cerebral cortical-ganglionic eminence fused organoids from patients with Timothy Syndrome in order to understand the effects of Timothy Syndrome on the developing cerebral cortex. Timothy Syndrome cerebral cortical-ganglionic eminence fused organoids show an increase in the saltatory migration frequency, but a decrease in the saltatory migration length, of GABAergic interneurons. In addition, Timothy Syndrome cerebral cortical-ganglionic eminence fused organoids show a decrease in the migration velocity of GABAergic interneurons, suggesting that Timothy Syndrome causes less effective GABAergic interneuron migration in the developing cerebral cortex (Birey et al., 2017). Following treatment with the l-type calcium channel blocker nimodipine, Timothy Syndrome cerebral cortical-ganglionic eminence fused organoids show similar saltation and migration patterns as wildtype cerebral cortical-ganglionic eminence fused organoids (Birey et al., 2017). Therefore, the utilization of organoid models to model the development of disorders in the nervous system may shed light on therapeutic treatments for disorders in the nervous system.

In our research, we generated a novel single-rosette organoid model to mimic the development and organization of the human cerebral cortex and human ganglionic eminences. Given that mouse models alone are insufficient in understanding the cellular mechanisms of PRE, our aims are to utilize cerebral cortical and ganglionic eminence single-rosette organoid models to understand the role of PCDH19 in the development of the brain, and therefore, the neurodevelopmental effects of PRE. Moreover, given that the current PRE therapies do not target the cellular mechanism of PRE, are insufficient in preventing seizures, and do not affect neurodevelopmental symptoms, our aims are to utilize our understanding of the cellular mechanisms of PRE to uncover novel therapeutic treatments for PRE.

MATERIALS AND METHODS

Preparation of Human Pluripotent Stem Cells

Human pluripotent stem cells were cultured on Geltrex, containing collagen, entactin, nidogen, laminin, heparin sulfate proteoglycans, and growth factors. 0.25ml Geltrex (Fisher, No. A1413302) was added to 25ml DMEM/F12 media (Invitrogen, No. 11330-032). Geltrex + DMEM/F12 media was added to each well in a 12-well plate. The 12-well plate was incubated at 37°C overnight.

Human pluripotent stem cells were added to the Geltrex + DMEM/F12 12-well plate. 10μM ROCK inhibitor (Cayman, No. 100005583) was added to TeSR-E8 media (StemCell Technology, No. 05940). ROCK inhibitor + TeSR-E8 media was added to each well for 24 hours. Then, TeSR-E8 media, without ROCK inhibitor, was added to each well daily, until the human pluripotent stem cell colonies reached desired confluence.

Once the human pluripotent stem cell colonies reached desired confluence, differentiated cells were removed with a 20μl pipet tip. TeSR-E8 media was aspirated from each well. Then, 1xDPBS was added to wash each well. Then, 1mM EDTA media (AccuGene, No. 51201) was added to each well for 2 minutes. EDTA media induced the separation of the human pluripotent stem cells from the colony. EDTA media was aspirated from each well. Then, TeSR-E8 media was added to each well for 2 minutes. The human pluripotent stem cells were passaged from the old Geltrex + DMEM/F12 12-well plate into the new Geltrex + DMEM/F12 12-well plate. ROCK inhibitor + TeSR-E8 media was added to each well for 24 hours. Then, TeSR-E8 media, without ROCK inhibitor, was added to each well daily.

Generation of Cerebral Cortical (Cortical) Organoids

Human pluripotent stem cells were cultured in three conditions. In condition one, wildtype H9 human stem cells virally labeled with GFP or RFP (or PCDH19-HA tag) were co-cultured in a one-to-one ratio. In condition two, *PCDH19* knockout human stem cells virally labeled with GFP or RFP (but not PCDH19-HA tag) were co-cultured in a one-to-one ratio. In condition three, wildtype H9 human stem cells virally labeled with RFP (or PCDH19-HA tag) and *PCDH19* knockout human stem cells virally labeled with GFP were co-cultured in a one-to-one ratio. The loss of PCDH19 in the *PCDH19* knockout human stem cells was confirmed previously. The addition of the PCDH19-HA tag in the wildtype human stem cells was

confirmed previously. Condition one was employed to model the development of the cerebral cortex in the healthy individual. Condition two was employed to model the development of the cerebral cortex in the male carrier. Condition three was employed to model the development of the cerebral cortex in the female PRE patient.

H9 human stem cells were cultured on Geltrex + DMEM/F12 12-well plates. On Day 0, 3N media (50:50 DMEM/F12:neurobasal (Fisher, No. 21103-049) with N2 (Fisher, No. 17502-048) and B27 (Fisher, No. 12587010) supplements without Vitamin A) with 3 inhibitors (2 μM DMH1 (Tocris, No. 4126), 2 μM XAV939 (Cayman, No. 13596), and 10 μM SB431542 (Cayman, No. 13031)) was added to each well. On Day 1, 3N media with 4 inhibitors (2 μM DMH1, 2 μM XAV939, 10 μM SB431542, and 1 μM cyclopamine (Cayman, No. 4449-51-8) was added to each well. At this time, the cells underwent differentiation, forming neuroepithelial sheets. On Day 5, neuroepithelial sheets were cut and passaged onto 100% Geltrex-coated vessels and cultured in 3N media with 4 inhibitors. On Day 7, 1 μM of WNT pathway activator CHIR99021 (Cayman, No. 13122) was added to each well. At this time, the neurons underwent polarization, forming a rosette structure with an apical membrane and a basal membrane. On Day 12, cortical organoids were "blown off" of Geltrex onto a low attachment U-bottom 96-well plate (one organoid in each well) with a STRIPPER PGD pipette. 3N media with Vitamin A, 20ng/ml BDNF (PeproTech, No. 450-02) and 20ng/ml NT3 (PeproTech, No. 450-03) was added to each well. Following Day 13, the cortical organoids formed an apical-basal structure that is similar to the human embryonic cerebral cortex *in vivo*, with a lumen, a ventricular zone, a subventricular zone, and a cortical plate. From Day 21 to Day 24, the cortical organoids were fixed and embedded in a cryomold, which was stored at -80°C.

Generation of Ganglionic Eminence (Ventral) Organoids

Human pluripotent stem cells were cultured in three conditions, similar to the conditions of the cortical organoids. In condition one, wildtype H9 human stem cells virally labeled with GFP or RFP were co-cultured in a one-to-one ratio. In condition two, *PCDH19* knockout human stem cells virally labeled with GFP or RFP were co-cultured in a one-to-one ratio. In condition three, wildtype H9 human stem cells virally labeled with GFP and *PCDH19* knockout human stem cells virally labeled with RFP were co-cultured in a one-to-one ratio. Condition one was employed to model the development of the ganglionic eminences in the healthy individual.

Condition two was employed to model the development of the ganglionic eminences in the male carrier. Condition three was employed to model the development of the ganglionic eminences in the female PRE patient.

H9 human stem cells were cultured on Geltrex + DMEM/F12 12-well plates. On Day 0, 3N media (without Vitamin A) with 3 inhibitors (2 μM DMH1, 2 μM XAV939, and 10 μM SB431542) was added to each well. At this time, the cells underwent differentiation, forming neuroepithelial sheets. On Day 5, neuroepithelial sheets were cut and passaged onto 100% Geltrex-coated vessels and cultured in 3N media with 3 inhibitors. On Day 7, 3N media with 1μM SAG (SelleckChem, No. S7779) and 2μM XAV939 was added to each well. At this time, the neurons underwent polarization, forming a rosette structure with an apical membrane and a basal membrane. On Day 12, ventral organoids were "blown off" of Geltrex onto a low attachment U-bottom 96-well plate (one organoid in each well) with a STRIPPER PGD pipette. On Day 15, 3N media with Vitamin A, 20ng/ml BDNF and 20ng/ml NT3 was added to each well was added to each well. On Day 34, the ventral organoids were fixed and embedded in a cryomold, which was stored at -80°C.

Immunocytochemistry Analysis

The cortical organoids and ventral organoids were sectioned with a cryostat into 20μm sections, which were mounted onto slides. The slides were washed with 1xPBS three times, each time for 5 minutes. Then, the slides were washed with 1xPBS and 0.2% Triton X-100 for 20 minutes. Then, the slides were washed with a blocking buffer, composed of 1xPBS, 0.05% Tween-20, and 5% Goat Serum, for 60 minutes (overnight for Day 6 and Day 12 whole-organoid staining). The slides were incubated with primary antibodies in Blocking Buffer, in their respective dilutions, in a cold room overnight (over two nights for Day 6 and Day 12 whole-organoid staining). Then, the slides were washed with 1xPBS and 0.05% Tween-20 three times, each time for 10 minutes. The slides were incubated with Alexa Fluor® dye conjugated secondary antibodies in blocking buffer, in a 1:400 dilution, for 90 minutes (overnight for Day 6 and Day 12 whole-organoid staining). Then, the slides were incubated with nuclear Bisbenzimide (BB) dye for 5 min (1 hour for Day 6 and Day 12 whole-organoid staining), followed by three washes with 1X PBS. The slides were mounted with glycegel, covered with coverslips, cured 1-2 days at room temperature, and were stored at -20°C.

Microscopy and Image Analysis

The cortical organoid and ventral organoid cryosections were imaged with an EVOS Fluorescent Microscope. The fluorescence was analyzed in 4 different channels: 405nm (blue), 488nm (green), 594nm (red), and 647nm (magenta). The brightness and contrast were adjusted with Image J. The images were organized with PowerPoint. The intensity was measured with Image J. The data were graphed with GraphPad Prism 8. A nonparametric unpaired t-test, as well as a Mann-Whitney significance test at a 95% confidence level, were utilized to determine statistical significance with GraphPad Prism 8. The error bar is presented as standard error of mean (SEM).

RESULTS

Generation of Cerebral Cortical (Cortical) Organoids & Ganglionic Eminence (Ventral) Organoids

In order to model the development and organization of the cerebral cortex and the ganglionic eminences, we generated cortical organoids and ventral organoids, respectively. Between Day 0 and Day 4, the human pluripotent stem cells underwent differentiation into excitatory cortical neuron progenitors and inhibitory ventral interneuron progenitors, forming cortical and ventral neuroepithelial monolayers (Fig. 1A). On Day 5, the cortical and ventral neuroepithelial monolayers were cut and passaged onto 100% Geltrex-coated vessels (not shown in Fig. 1A). Between Day 5 and Day 11, the cortical neurons and ventral neurons underwent polarization into neural rosettes (Fig. 1A). Finally, following Day 12, the cortical and ventral organoids were "blown off" of Geltrex vessels onto low attachment U-bottom 96-well plates (one organoid in each well), at which time the cortical organoids and ventral organoids formed structures similar to the early fetal stages of the human cerebral cortex and human ganglionic eminences *in vivo* (Fig. 1A and B).

In order to confirm the generation of cortical organoids and ventral organoids, we employed immunocytochemistry to image the expression of cerebral cortical and ganglionic eminence markers. At Day 24, the cortical organoids were fixed, sectioned, and stained with antibodies against SOX2, a cerebral cortical neural stem cell marker. At this time, the cortical organoids showed strong expression of SOX2 (Fig. 1B). At Day 34, the ventral organoids were fixed, sectioned, and stained with antibodies against NKX2.1, a ganglionic eminence neural stem cell marker. At this time, the ventral organoids showed strong expression of NKX2.1 (Fig. 1B).

Generation of Cortical Organoids in Healthy, Carrier, and PRE Conditions

In order to model the development and organization of the cerebral cortex in healthy individuals, male carriers, and female PRE patients, we generated wildtype-wildtype "healthy" cortical organoids, *PCDH19* knockout-knockout "carrier" cortical organoids, and wildtype-*PCDH19* knockout "PRE" cortical organoids, respectively. In the wildtype-wildtype "healthy" cortical organoids, we labeled wildtype (PCDH19-positive) cells with GFP or RFP; in the *PCDH19* knockout-knockout "carrier" cortical organoids, we labeled PCDH19-negative cells with GFP or RFP; and in the wildtype-*PCDH19* knockout "PRE" cortical organoids, we labeled

PCDH19-positive cells with RFP and PCDH19-negative cells with GFP. In this way, we were able to track how PCDH19-positive cells interact with PCDH19-mutant cells in live imaging. Furthermore, to understand the cellular mechanism of PRE, we employed live imaging to image the organization of cells in "healthy" cortical organoids, "carrier" cortical organoids, and "PRE" cortical organoids. At Day 15, the "healthy" cortical organoids, "carrier" cortical organoids, and "PRE" cortical organoids showed similar morphologies. All three types of cortical organoids showed an even distribution of cells (Fig. 2A). At Day 17, the "healthy" cortical organoids, "carrier" cortical organoids, and "PRE" cortical organoids showed different morphologies. Whereas the "healthy" cortical organoids and "carrier" cortical organoids showed a uniform distribution of cells, the "PRE" cortical organoids showed an uneven distribution of PCDH19-positive and PCDH19-negative cells (Fig. 2B). In the "PRE" cortical organoids, PCDH19-positive cells and PCDH19-negative cells were segregated to distinct areas of the cortical organoid (Fig. 2B and C). At Day 24, the "PRE" cortical organoids showed a similar, but more severe segregation phenotype (Fig. 2C).

Comparison of Cortical Organoids Between Healthy and PRE Conditions

To understand the role of PCDH19 on the development of the cerebral cortex, as well as the neurodevelopmental effects of PRE, we employed immunocytochemistry to image the expression of cerebral cortical developmental markers in "healthy" cortical organoids and "PRE" cortical organoids. At Day 24, the "healthy" cortical organoids and "PRE" cortical organoids were fixed, sectioned, and stained with antibodies against NCAD, a cadherin expressed at the apical lumen. At this time, both the "healthy" cortical organoids and "PRE" cortical organoids showed strong expression of NCAD at the lumen, resembling the ventricular surface in the cerebral cortex *in vivo* (Fig. 3). Additionally, at Day 24, the "healthy" cortical organoids and "PRE" cortical organoids were fixed, sectioned, and stained with antibodies against SOX2, an apical radial glial cell marker of the ventricular zone, pVIM, a dividing radial glial cell marker, and TBR2, an intermediate progenitor cell marker of the subventricular zone. At this time, both the "healthy" cortical organoids and "PRE" cortical organoids showed strong expression of SOX2 and pVIM in the ventricular-like zone and TBR2 in the subventricular-like zone, indicating the presence of dividing apical radial glial cells in the ventricular-like zone and intermediate progenitor cells in the subventricular-like zone, resembling the ventricular zone and

subventricular zone in the cerebral cortex *in vivo* (Fig. 3). Finally, at Day 24, the "healthy" cortical organoids and "PRE" cortical organoids were fixed, sectioned, and stained with antibodies against CTIP2, a deep layer neuronal marker of the cortical plate. At this time, both the "healthy" cortical organoids and "PRE" cortical organoids showed strong expression of CTIP2 in periphery of the organoids, indicating the presence of neurons in the periphery of the organoids, resembling the cortical plate in the cerebral cortex *in vivo* (Fig. 3).

To better understand the neurodevelopmental effects of PRE, we employed intensity analyses to measure the expression of specific cerebral cortical developmental markers in "healthy" cortical organoids and "PRE" cortical organoids. Previous studies have shown that PCDH19 interacts with NCAD through a cis interface, forming a PCDH19-NCAD dimer (Gerosa et al., 2019). At Day 6, while the cortical organoids were embedded in Geltrex, "healthy" cortical organoids and "PRE" cortical organoids were stained with antibodies against NCAD. At this time, it is important to note that the "PRE" cortical organoids seemed to show more intense NCAD expression than the "healthy" cortical organoids (Fig. 4A). We measured the intensity of NCAD expression and Bisbenzimide (BB) in 5 "healthy" cortical organoids and 3 "PRE" cortical organoids. According to the intensity analyses, the "PRE" cortical organoids showed an average NCAD:BB intensity ratio of 0.222, whereas the "healthy" cortical organoids showed an average intensity ratio of 0.157; however, the difference was insignificant at the 95% confidence level (Fig. 4B). Again, at Day 12, while the cortical organoids were embedded in Geltrex, "healthy" cortical organoids and "PRE" cortical organoids were stained with antibodies against NCAD. In contrast, at this time it is important to note that the "healthy" cortical organoids seemed to show more intense NCAD expression than the "PRE" cortical organoids (Fig. 5A). We measured the intensity of NCAD expression and Bisbenzimide (BB) in 4 "healthy" cortical organoids and 5 "PRE" cortical organoids. According to the intensity analyses, the "healthy" cortical organoids showed an average NCAD:BB intensity ratio of 0.330, whereas the "PRE" cortical organoids showed an average intensity ratio of 0.252. The difference was significant at the 95% confidence interval (p-value of 0.0317) (Fig. 5B); however, additional biological replicates are required for further validation. Additionally, at Day 21, after the cortical organoids were "blown off" of Geltrex, "healthy" cortical organoids and "PRE" cortical organoids were fixed, sectioned, and stained with antibodies against NCAD. At this time, the "PRE" cortical organoids showed segregation of PCDH19-positive cells from PCDH19-negative

cells. It is important to note that the PCDH19-positive cells seemed to show more intense NCAD expression than the PCDH19-negative cells in the “PRE” cortical organoids (Fig. 6A). We measured the intensity of NCAD expression and Bisbenzimide (BB) in 5 PCDH19-positive cell areas and 4 PCDH19-negative cell areas in 1 “PRE” cortical organoid. According to the intensity analyses, the PCDH19-positive cell areas showed an average NCAD:BB intensity ratio of 0.757, whereas the PCDH19-negative cell areas showed an average intensity ratio of 0.346 (Fig. 6B). However, we were unable to perform statistical testing with one replicate, we require additional biological replicates.

Furthermore, at Day 21, “healthy” cortical organoids and “PRE” cortical organoids were fixed, sectioned, and stained with antibodies against TBR2. At this time, it is important to note that the “healthy” cortical organoids seemed to show more intense TBR2 expression than the “PRE” cortical organoids (Fig. 7A). We measured the intensity of TBR2 expression and Bisbenzimide (BB) in the ventricular-like zone/subventricular-like zone and cortical plate-like area in 10 “healthy” cortical organoids and 2 “PRE” cortical organoids. According to the intensity analyses, the “healthy” cortical organoids showed an average TBR2:BB intensity ratio of 0.347 in the ventricular-like zone/subventricular-like zone, whereas the “PRE” cortical organoids showed an average intensity ratio of 0.177 in the ventricular-like zone/subventricular-like zone; however, the difference was insignificant at the 95% confidence level, likely due to the small sample size of the “PRE” cortical organoids (Fig. 7B). In addition, the “healthy” cortical organoids showed an average TBR2:BB intensity ratio of 0.426 in the cortical plate-like area, whereas the “PRE” cortical organoids showed an average intensity ratio of 0.137 in the cortical plate-like area; however, the difference was insignificant at the 95% confidence level, likely due to the small sample size of the “PRE” cortical organoids (Fig. 7C).

Moreover, at Day 21, “healthy” cortical organoids and “PRE” cortical organoids were fixed, sectioned, and stained with antibodies against CTIP2. In contrast, at this time, it is important to note that the “PRE” cortical organoids seemed to show more intense CTIP2 expression than the “healthy” cortical organoids (Fig. 8A). We measured the intensity of CTIP2 expression and Bisbenzimide (BB) in the ventricular-like zone/subventricular-like zone and cortical plate-like area in 10 “healthy” cortical organoids and 2 “PRE” cortical organoids. According to the intensity analyses, the “PRE” cortical organoids showed an average CTIP2:BB intensity ratio of 0.853 in the ventricular-like zone/subventricular-like zone, whereas the

"healthy" cortical organoids showed an average intensity ratio of 0.709 in the ventricular-like zone/subventricular-like zone; however, the difference was insignificant at the 95% confidence level, likely due to the small sample size of the "PRE" cortical organoids (Fig. 8B). Nonetheless, the "healthy" cortical organoids showed an average CTIP2:BB intensity ratio of 0.605 in the cortical plate-like area, whereas the "PRE" cortical organoids showed an average intensity ratio of 0.777 in the cortical plate-like area; however, the difference was insignificant at the 95% confidence level, likely due to the small sample size of the "PRE" cortical organoids (Fig. 8C).

Generation of Ventral Organoids in Healthy, Carrier, and PRE Conditions

In order to model the development and organization of the ganglionic eminences in healthy individuals, male carriers, and female PRE patients, we generated wildtype-wildtype "healthy" ventral organoids, *PCDH19* knockout-knockout "carrier" ventral organoids, and wildtype-*PCDH19* knockout "PRE" ventral organoids, respectively. In the wildtype-wildtype "healthy" ventral organoids, we labeled wildtype (PCDH19-positive) cells with GFP or RFP; in the *PCDH19* knockout-knockout "carrier" ventral organoids, we labeled PCDH19-negative cells with GFP or RFP; and in the wildtype-*PCDH19* knockout "PRE" ventral organoids, we labeled PCDH19-positive cells with GFP and PCDH19-negative cells with RFP. Furthermore, to understand the cellular mechanism of PRE, we employed live imaging to image the organization of cells in "healthy" ventral organoids, "carrier" ventral organoids, and "PRE" ventral organoids. At Day 13, the "healthy" ventral organoids, "carrier" ventral organoids, and "PRE" ventral organoids showed similar morphologies. All three types of ventral organoids showed an even distribution of cells (Fig. 9A). At Day 18, the "healthy" ventral organoids, "carrier" ventral organoids, and "PRE" ventral organoids showed different morphologies. Whereas the "healthy" ventral organoids and "carrier" ventral organoids showed a uniform distribution of cells, the "PRE" ventral organoids showed an uneven distribution of PCDH19-positive and PCDH19-negative cells (Fig. 9B). In the "PRE" ventral organoids, PCDH19-positive cells and PCDH19-negative cells were segregated to distinct areas of the ventral organoid – PCDH19-positive cells to the inner area of the ventral organoid and PCDH19-negative cells to the outer area of the ventral organoid (Fig. 9B and C). At Day 24, the "PRE" ventral organoids showed a similar, but more severe segregation phenotype (Fig. 9C).

Comparison of Ventral Organoids Between Healthy and PRE Conditions

To understand the role of PCDH19 on the development of the ganglionic eminences, as well as the neurodevelopmental effects of PRE, we employed immunocytochemistry to image the expression of ganglionic eminence developmental markers in “healthy” ventral organoids and “PRE” ventral organoids. At Day 34, the “healthy” ventral organoids and “PRE” ventral organoids were fixed, sectioned, and stained with antibodies against KI67, a proliferative cell marker. At this time, both the “healthy” ventral organoids and “PRE” ventral organoids showed strong expression of KI67, indicating the presence of proliferative cells, resembling the ganglionic eminences *in vivo* (Fig. 10). Additionally, at Day 34, the “healthy” ventral organoids and “PRE” ventral organoids were fixed, sectioned and stained with antibodies against TuJ1, a neuronal marker. At this time, both the “healthy” ventral organoids and “PRE” ventral organoids showed strong expression of TuJ1, indicating the presence of neurons, resembling the ganglionic eminences *in vivo* (Fig. 10). Given that we did not have Bisbenzimide (BB) staining, we were unable to do relative intensity analyses.

DISCUSSION

Per the comparison of wildtype-wildtype "healthy" cortical organoids, *PCDH19* knockout-knockout "carrier" cortical organoids, and wildtype-*PCDH19* knockout "PRE" cortical organoids, we are able to identify distinct phenotypic differences in the "PRE" cortical organoids as compared to the "healthy" and "carrier" cortical organoids. Likewise, per the comparison of wildtype-wildtype "healthy" ventral organoids, *PCDH19* knockout-knockout "carrier" ventral organoids, and wildtype-*PCDH19* knockout "PRE" ventral organoids, we are able to identify distinct phenotypic differences in the "healthy" and "carrier" ventral organoids, as compared to the "PRE" ventral organoids. In the "healthy" organoids, the PCDH19-positive cells show the expected pattern of cell mixing. Similarly, in the "carrier" organoids, the PCDH19-negative cells show the expected pattern of cell mixing. This suggests that the PCDH19-positive cells have similar adhesion properties and PCDH19-negative cells have similar adhesion properties (Dibbens et al., 2008). Conversely, in the "PRE" organoids, the PCDH19-positive cells and PCDH19-negative cells show abnormal cell sorting. This finding suggests that the PCDH19-positive cells and PCDH19-negative cells have different adhesion properties. In addition, this finding suggests that the PCDH19-positive cells have repulsive chemoaffinity labels for PCDH19-negative cells, and the PCDH19-negative cells have repulsive chemoaffinity labels for PCDH19-positive cells (Dibbens et al., 2008). Therefore, our findings suggest that the cellular interference of PCDH19 is the cellular mechanism of PRE, as described in previous studies (Dibbens et al., 2008; Pederick et al., 2018).

Furthermore, per the comparison of "healthy" cortical organoids and "PRE" cortical organoids, we are able to speculate that "PRE" cortical organoids have an abnormal cytoarchitecture as compared to "healthy" cortical organoids. At Day 12, prior to the segregation of PCDH19-positive cells from PCDH19-negative cells in the "PRE" cortical organoids, the "PRE" cortical organoids show significantly less intense NCAD expression than the "healthy" cortical organoids. Likewise, at Day 21, following the segregation of PCDH19-positive cells from PCDH19-negative cells in the "PRE" cortical organoids, the PCDH19-negative areas of the "PRE" cortical organoids show significantly less intense NCAD expression than the PCDH19-positive areas of the "PRE" cortical organoids. Given that PCDH19 interacts with NCAD through a cis interface, forming a PCDH19-NCAD dimer, our results suggest that PCDH19 presence or absence may affect NCAD expression or subcellular distribution (Gerosa et al.,

2019). Additionally, at Day 21, the "PRE" cortical organoids show notably, albeit insignificantly, less intense TBR2 expression in the ventricular-like zone/subventricular-like zone and the cortical plate-like area than the "healthy" cortical organoids. It is important to note that whereas "healthy" cortical organoids show notably less intense TBR2 expression in the ventricular-like zone/subventricular-like zone as compared to the cortical plate-like area, "PRE" cortical organoids show notably more intense TBR2 expression in the ventricular-like zone/subventricular-like zone as compared to the cortical plate-like area. Given that TBR2 is an intermediate progenitor cell marker, our results speculate either that "PRE" cortical organoids encounter less intermediate progenitor cell expansion than "healthy" cortical organoids or that "PRE" cortical organoids encounter more premature differentiation than "healthy" cortical organoids. Finally, at Day 21, the "PRE" cortical organoids show notably, albeit insignificantly, more intense CTIP2 expression in the ventricular-like zone/subventricular-like zone than the "healthy" cortical organoids; however, the "PRE" cortical organoids show notably, albeit insignificantly, less intense CTIP2 expression in the cortical plate-like area than the "healthy" cortical organoids. It is important to note that whereas "healthy" cortical organoids show notably less intense CTIP2 expression in the ventricular-like zone/subventricular-like zone as compared to the cortical plate-like area, "PRE" cortical organoids show notably more intense CTIP2 expression in the ventricular-like zone/subventricular-like zone as compared to the cortical plate-like area. Given that CTIP2 is a deep laminal neuronal marker, our results speculate either that "PRE" cortical organoids encounter less neuronal expansion than "healthy" cortical organoids or that "PRE" cortical organoids encounter more premature neuronal differentiation than "healthy" cortical organoids. Therefore, our results suggest that "PRE" cortical organoids have an abnormal cortical lamination, although a similar pattern has not been identified in PRE patients yet.

Moreover, per the comparison of "healthy" ventral organoids and "PRE" ventral organoids, we are able to speculate that "PRE" ventral organoids have an abnormal cytoarchitecture as compared to "healthy" ventral organoids. At Day 34, the "PRE" ventral organoids show seemingly less intense KI67 expression than the "healthy" ventral organoids. Given that KI67 is a proliferative cell marker, our results speculate that "PRE" ventral organoids encounter less cell proliferation than wildtype-wildtype ventral organoids. Additionally, at Day 34, the "PRE" ventral organoids show seemingly more intense TuJ1 expression than the

"healthy" ventral organoids. Given that TuJ1 is a neuronal marker, our results speculate that "PRE" ventral organoids have more premature neuronal differentiation than "healthy" ventral organoids. However, more analyses need to be conducted in the future.

Nonetheless, it is important to note that our results have limited statistical power. We have a limited amount of immunocytochemistry and intensity analyses in cortical and ventral organoids. In order to move from speculation to conclusion, we have to carry out additional experiments in the future.

Conclusion

In conclusion, our data shows that wildtype-wildtype "healthy" organoids, *PCDH19* knockout-knockout "carrier" organoids, and wildtype-*PCDH19* knockout "PRE" organoids are effective models of the development and organization of the brain in healthy individuals, male carriers, and female PRE patients, respectively. The "healthy" organoids show cell mixing, similar to the phenotype of healthy individuals. Similarly, the "carrier" organoids show cell mixing, similar to the phenotype of male carrier patients. Conversely, the "PRE" organoids show cell segregation, and abnormal cytoarchitecture, indicating potential abnormal phenotypes of PRE during the development of the brain. Future research should focus on investigating the cellular mechanism of PRE in further detail, such as discovering the mechanism of the interaction of PCDH19 wildtype cells and mutant cells in PRE, identifying seizure-like phenotypes of PRE, and investigating network activity in cortical-ventral fused organoids. Our results show that modeling PRE in organoids can provide insights into the cellular mechanism of PRE. In addition, as we were able to identify robust phenotypes of PRE in organoids, PRE organoids could be a powerful platform for drug screening for PRE in future.

REFERENCES

Birey F, Andersen J, Makinson C, Islam S, Wei W, Huber N, Fan H, Metzler K, Panagiotakos G, Thom N, O'Rourke N, Steinmetz L, Bernstein J, Hallmayer J, Huguenard J, Pasca S (2017) Assembly of functionally integrated human forebrain spheroids. Nature 545:54-59.

Depienne C et al. (2009) Sporadic infantile epileptic encephalopathy caused by mutations in PCDH19 resembles dravet syndrome but mainly affects females. PLOS Genetics 5:e1000381.

Dibbens L et al. (2008) X-linked protocadherin 19 mutations cause female-limited epilepsy and cognitive impairment. Nature Genetics 40:776-781.

Gerosa L, Francolini M, Bassani S, Passafaro M (2019) The role of rotocadherin 19 (PCDH19) in neurodevelopment and in the pathophysiology of early infantile epileptic encephalopathy-9 (EIEE9). Developmental Neurobiology 79:75-84.

Hansen D, Lui J, Parker P, Kriegstein A (2010) Neurogenic radial glia in the outer subventricular zone of human neocortex. Nature 464:554-561.

Herculano-Houzel S (2009) The human brain in numbers: A linearly scaled-up primate brain. Frontiers in Human Neuroscience 3:31.

Juberg R, Hellman C (1971) A new familial form of convulsive disorder and mental retardation limited to females. Journal of Pediatrics 79:726-732.

Kim S, Chung H, Sun W, Kim H (2007) Spatiotemporal expression pattern of non-clustered protocadherin family members in the developing rat brain. Neuroscience 147:996-1021.

Knight G, Lundin B, Iyer N, Ashton L, Sethares W, Willett R, Ashton, R (2018) Engineering induction of singular neural rosette emergence within hPSC-derived tissues. eLife 7:e37549.

Kolc K, Sadleir L, Scheffer I, Ivancevic A, Roberts R, Pham D, Gecz J (2019) A systemic review and meta-analysis of 271 PCDH19-variant individuals identifies psychiatric comorbidities, and association of seizure onset and disease severity. Molecular Psychiatry 24:241-251.

Liu Y, Liu H, Sauvey C, Yao L, Zarnowska E, Zhang S (2013) Directed differentiation of forebrain GABA interneurons from human pluripotent stem cells. Nature Protocols 8:1670-1679.

Okita K, Ichisaka T, Yamanaka S (2007) Generation of germline-competent induced pluripotent stem cells. Nature 448:313-317.

Pederick D, Richards K, Piltz S, Kumar R, Mincheva-Tasheva S, Mandelstam S, Dale R, Scheffer I, Gecz J, Petrou S, Hughes J, Thomas P (2018) Abnormal cell sorting underlies the unique x-linked inheritance pattern of PCDH19 epilepsy. Neuron 97:59-66.

Scheffer I et al. (2008) Epilepsy and mental retardation limited to females: An under-recognized disorder. Brain 131:918-927.

Soriano E and Del Rio J (2005) The cells of cajal-retzius: Still a mystery one century after. Neuron 46:389-394.

Stoykova A, Hatano O, Gruss P, Gotz M (2003) Increase in reelin-positive cells in the marginal zone of pax6 mutant mouse cortex. Cerebral Cortex 13:560-571

Terracciano A, Trivisano M, Cusmai R, Palma L, Fusco L, Compagnucci C, Bertini E, Vigevano F, Specchio N (2016). PCDH19-related epilepsy in two mosaic male patients. Epilepsia 57:51-55.

Thiffault I, Farrow E, Smith L, Lowry J, Zellmer L, Black B, Abdelmoity A, Miller N, Soden S, Saunders C (2016) PCDH19-related epileptic encephalopathy in a male mosaic for a truncating variant. American Journal of Medical Genetics 170:1585-1589.

Watanabe M et al. (2017) Self-organized cerebral organoids with human-specific features predict effective drugs to combat zika virus infection. Cell Reports 21:517-532.

Xiang Y, Tanaka Y, Patterson B, Kang Y, Govindaiah G, Roselaar N, Cakir B, Kim K, Lombroso A, Hwang S, Zhong M, Stanley E, Elefanty A, Naegele J, Lee S, Weissman S, Park I (2017) Fusion of regionally specified hPSC-derived organoids models human brain development and interneuron migration. Cell Stem Cell 21:383-398.

Zecevic N, Chen Y, Filipovic R (2005) Contributions of cortical subventricular zone to the development of the human cerebral cortex. Journal of Comparative Neurology 491:109-122.

APPENDIX OF FIGURES

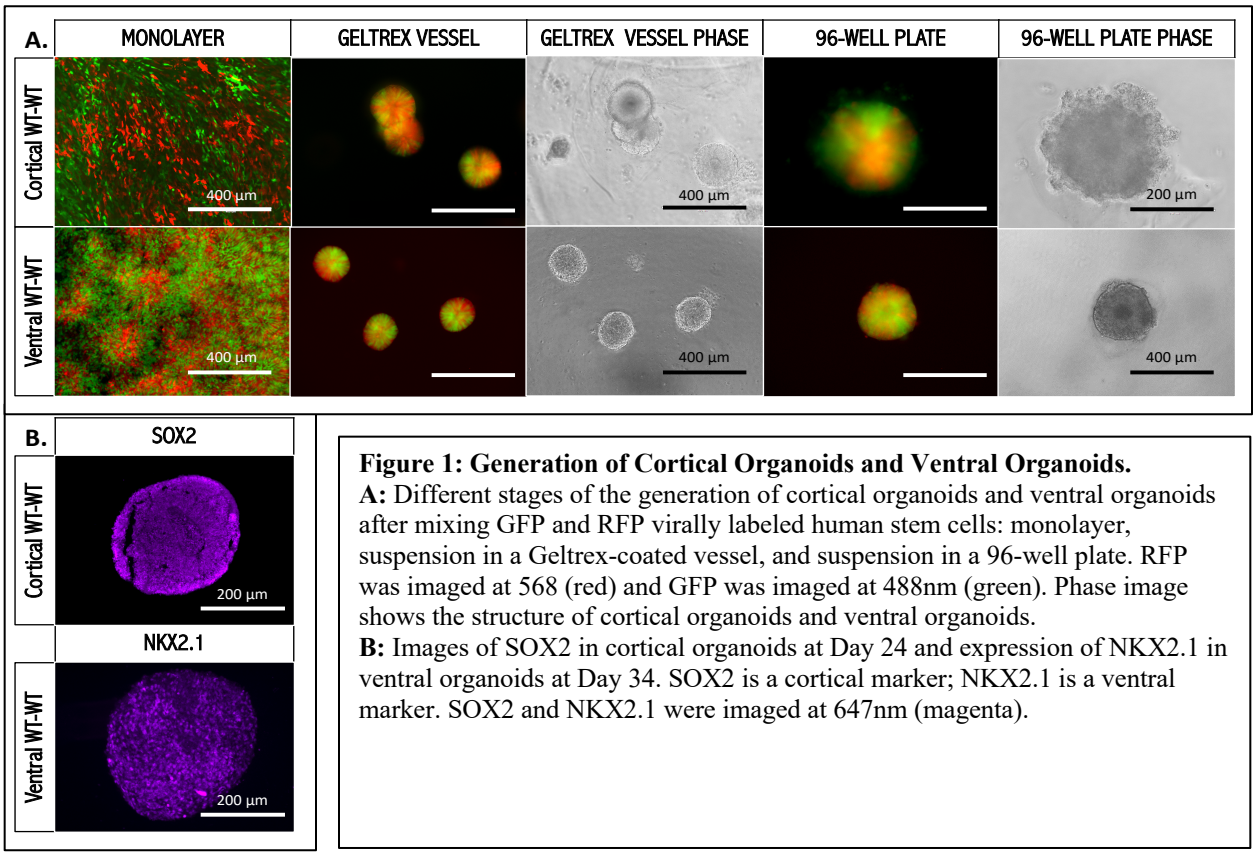

Figure 1: Generation of Cortical Organoids and Ventral Organoids.
A: Different stages of the generation of cortical organoids and ventral organoids after mixing GFP and RFP virally labeled human stem cells: monolayer, suspension in a Geltrex-coated vessel, and suspension in a 96-well plate. RFP was imaged at 568 (red) and GFP was imaged at 488nm (green). Phase image shows the structure of cortical organoids and ventral organoids.
B: Images of SOX2 in cortical organoids at Day 24 and expression of NKX2.1 in ventral organoids at Day 34. SOX2 is a cortical marker; NKX2.1 is a ventral marker. SOX2 and NKX2.1 were imaged at 647nm (magenta).

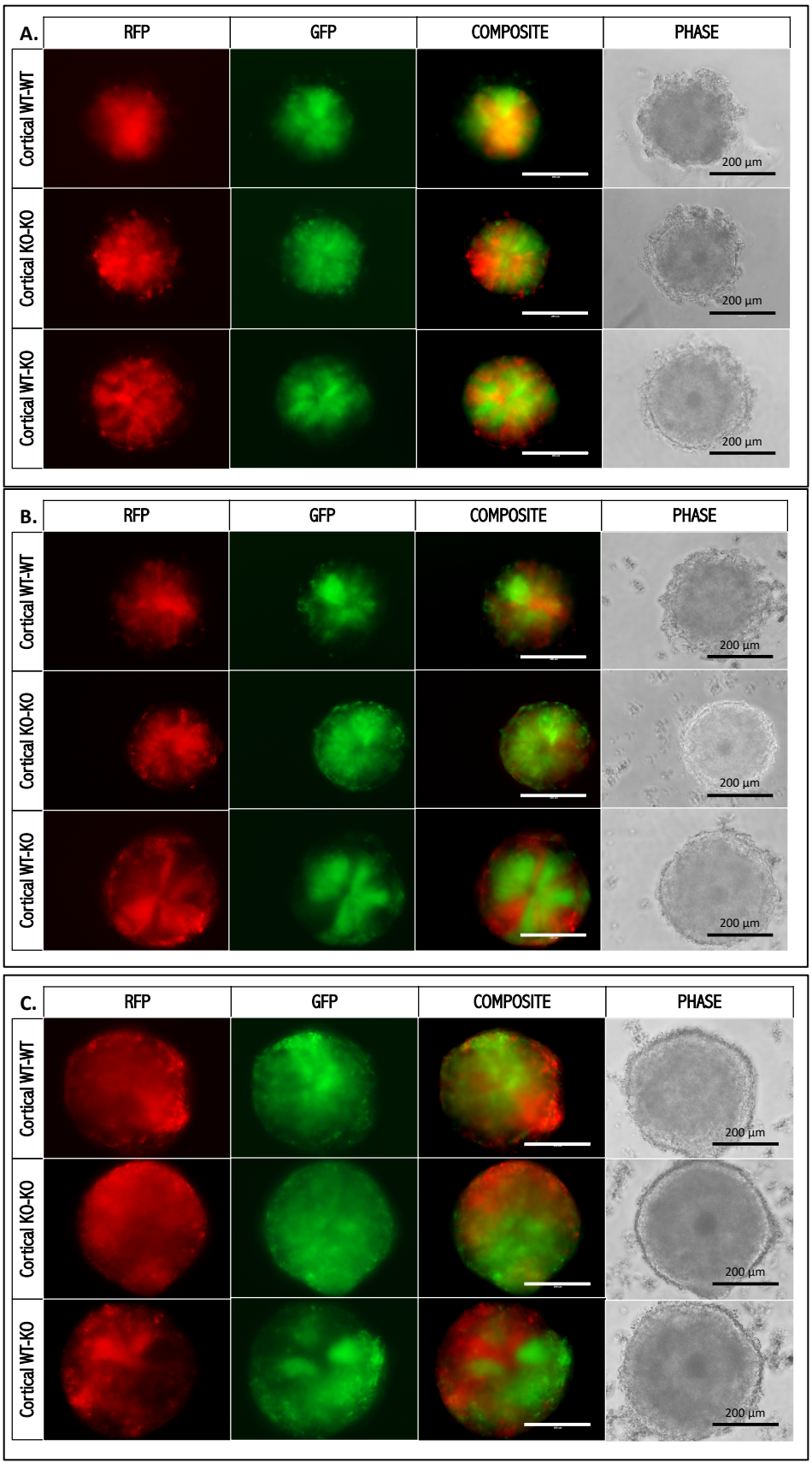

Figure 2: Live Imaging of RFP and GFP in Cortical Organoids at Days 15, 17, and 24. Images of RFP and GFP in "healthy" cortical organoids, "carrier" cortical organoids, and "PRE" cortical organoids at Days 15, 17, and 24. RFP was imaged at 568 (red) and GFP was imaged at 488nm (green). Phase image shows the structure of "healthy" cortical organoids, "carrier" cortical organoids, and "PRE" cortical organoids. The scale bar is 200 micrometers.
A: Images of RFP and GFP in "healthy" cortical organoids, "carrier" cortical organoids, and "PRE" cortical organoids at Day 15.
B: Images of RFP and GFP in "healthy" cortical organoids, "carrier" cortical organoids, and "PRE" cortical organoids at Day 17.
C: Images of RFP and GFP in "healthy" cortical organoids, "carrier" cortical organoids, and "PRE" cortical organoids at Day 24.

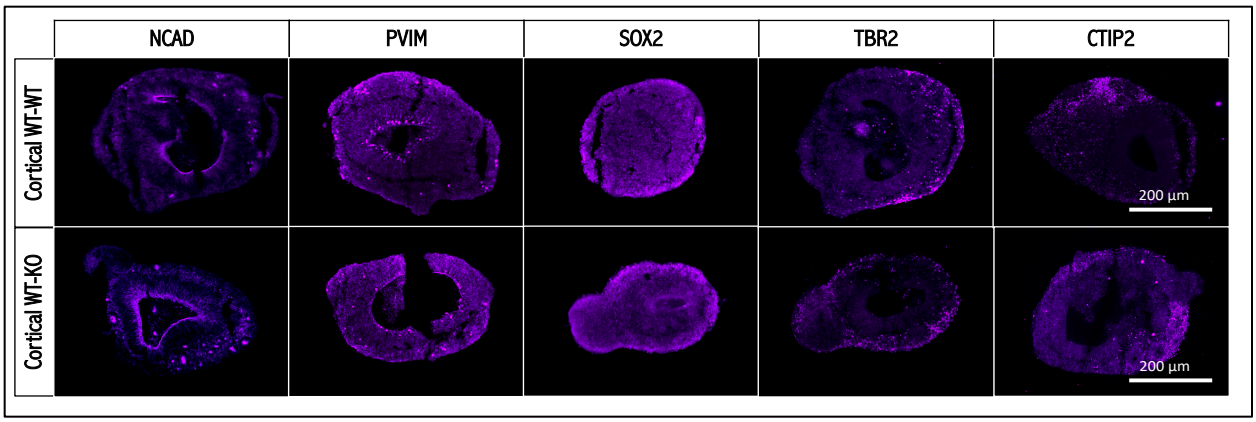

Figure 3: Immunocytochemistry of NCAD, pVIM, SOX2, TBR2, and CTIP2 in Cortical Organoids at Day 24.
Images of NCAD, pVIM, SOX2, TBR2, and CTIP2 in "healthy" cortical organoids and "PRE" cortical organoids at Day 24. NCAD outlines the lumen; pVIM is a dividing radial glial cell marker; SOX2 is an apical radial glial cell marker in the ventricular zone; TBR2 is an intermediate progenitor cell marker in the subventricular zone; and CTIP2 is a deep laminal neuronal marker in the cortical plate. NCAD, pVIM, SOX2, TBR2, and CTIP2 were imaged at 647nm (magenta). The scale bar is 200 micrometers.

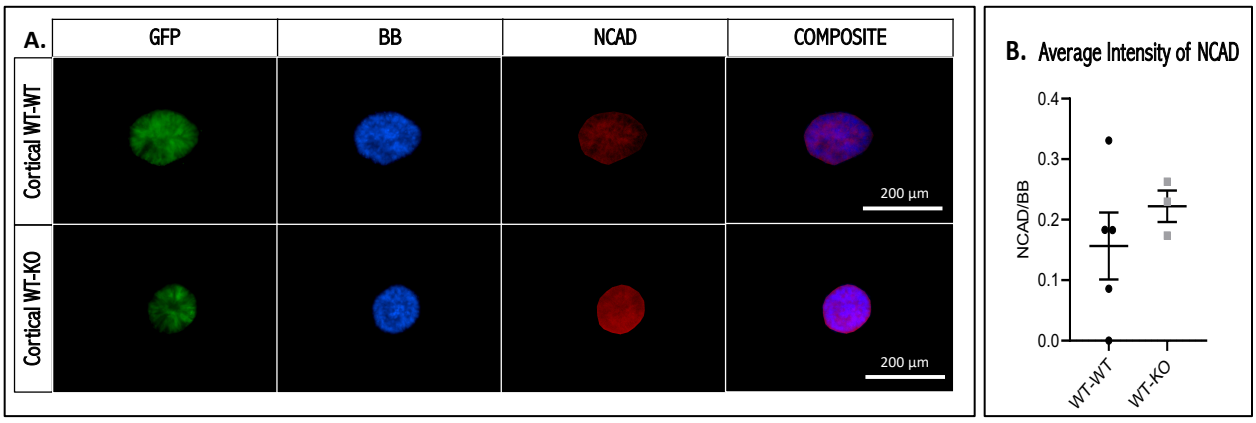

Figure 4: Immunocytochemistry and Quantification of NCAD in Cortical Organoids at Day 6.
A: Images of GFP, BB, and NCAD in "healthy" cortical organoids and "PRE" cortical organoids at Day 6. BB stains nuclei; NCAD outlines the lumen. BB and NCAD composite image shows the relative NCAD expression in "healthy" cortical organoids and "PRE" cortical organoids. GFP was imaged at 488nm (green), BB was imaged at 405nm (blue) and NCAD was imaged at 568nm (red). The scale bar is 200 micrometers.
B: Scatter plot of average NCAD:BB intensity ratio in "healthy" cortical organoids and "PRE" cortical organoids.

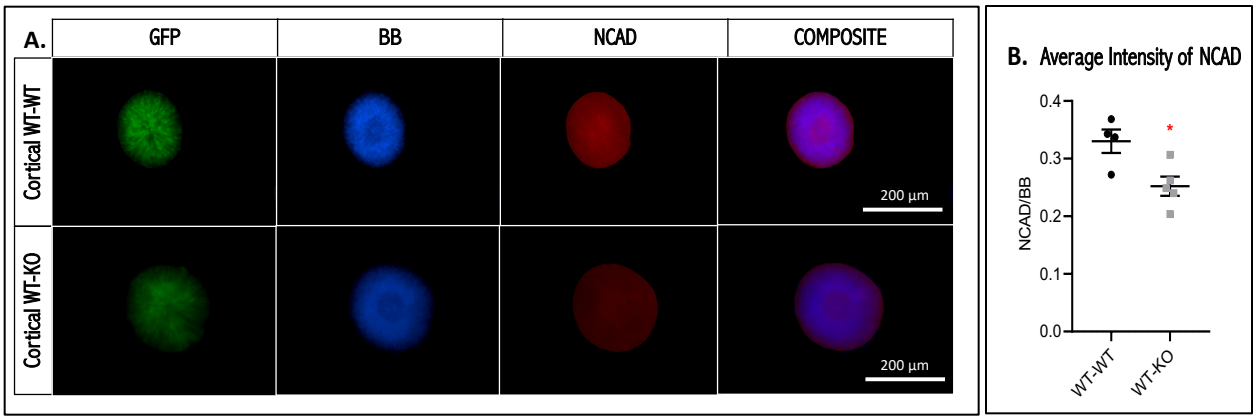

Figure 5: Immunocytochemistry and Quantification of NCAD in Cortical Organoids at Day 12.
A: Images of GFP, BB, and NCAD in "healthy" cortical organoids and "PRE" cortical organoids at Day 12. BB stains nuclei; NCAD outlines the lumen. BB and NCAD composite image shows the relative NCAD expression in "healthy" cortical organoids and "PRE" cortical organoids. GFP was imaged at 488nm (green), BB was imaged at 405nm (blue) and NCAD was imaged at 568nm (red). The scale bar is 200 micrometers.
B: Scatter plot of average NCAD:BB intensity ratio in "healthy" cortical organoids and "PRE" cortical organoids. * $p<0.05$.

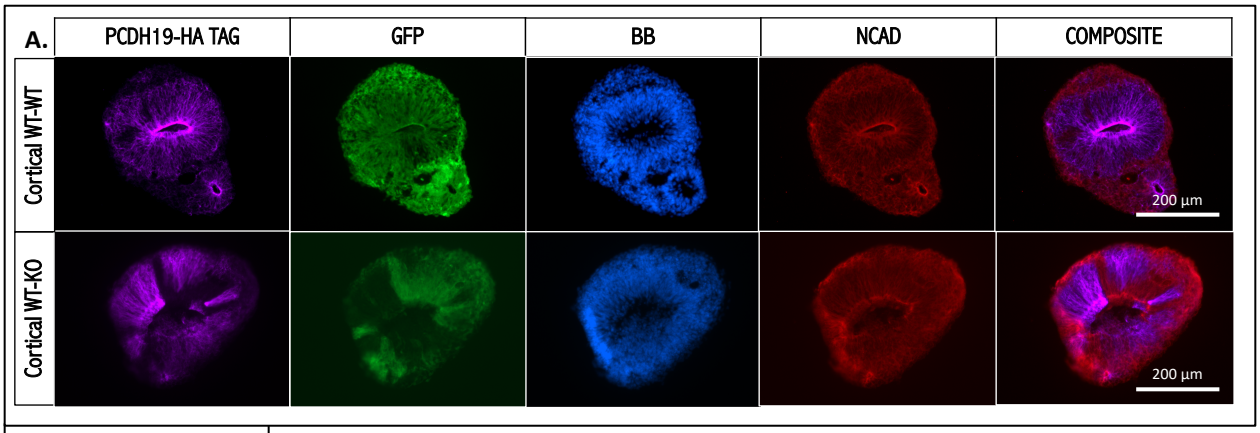

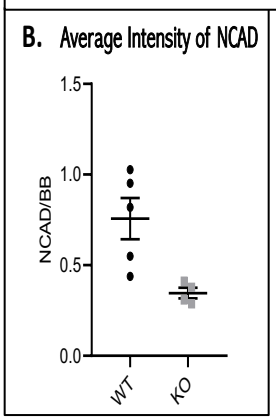

Figure 6: Immunocytochemistry and Quantification of NCAD in Cortical Organoids at Day 21.
A: Images of *PCDH19*-HA tag, GFP, BB, and NCAD in "healthy" cortical organoids and "PRE" cortical organoids at Day 21. BB stains nuclei; NCAD outlines the lumen. *PCDH19*-HA tag and NCAD composite image shows the relative NCAD expression in PCDH19-positive cells and PCDH19-negative cells in "healthy" cortical organoids and "PRE" cortical organoids. *PCDH19*-HA tag was imaged at 647nm (magenta), GFP was imaged at 488nm (green), BB was imaged at 405nm (blue), and NCAD was imaged at 568nm (red). The scale bar is 200 micrometers.
B: Scatter plot of average NCAD:BB intensity ratio in "healthy" cortical organoids and "PRE" cortical organoids.

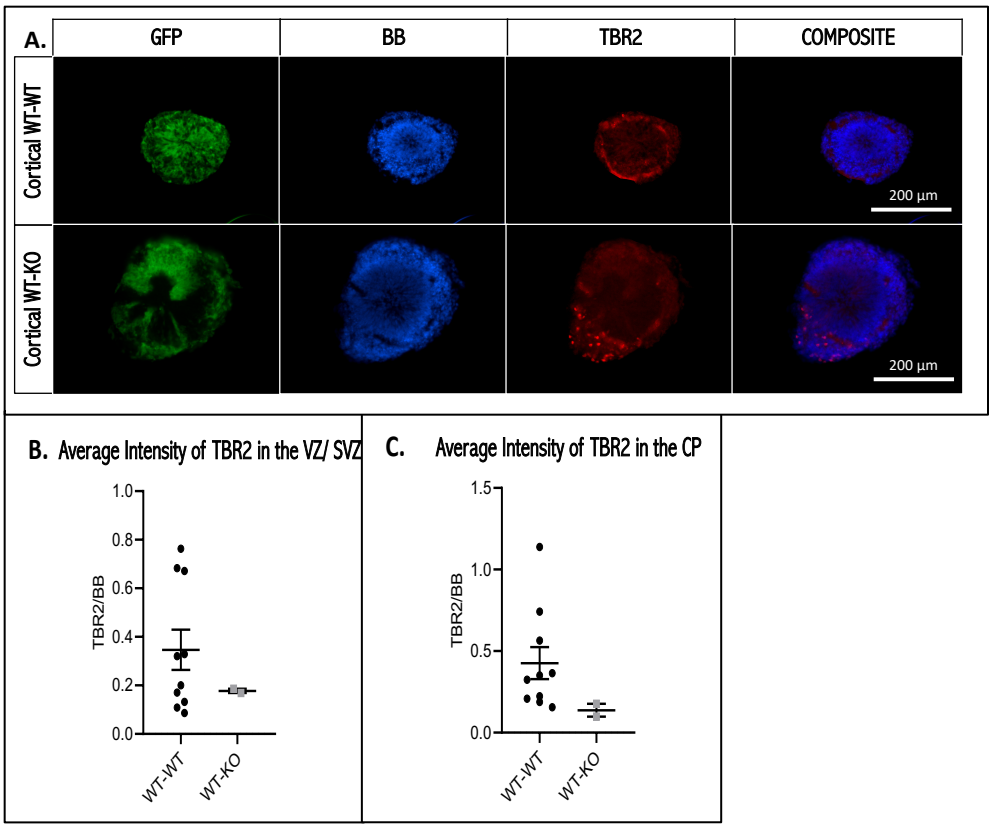

Figure 7: Immunocytochemistry and Quantification of TBR2 in Cortical Organoids at Day 21.
A: Images of GFP, BB, and TBR2 in "healthy" cortical organoids and "PRE" cortical organoids at Day 21. BB stains nuclei; TBR2 is an intermediate progenitor cell marker in the subventricular zone. BB and TBR2 composite image shows the relative TBR2 expression in "healthy" cortical organoids and "PRE" cortical organoids. GFP was imaged at 488nm (green), BB was imaged at 405nm (blue) and TBR2 was imaged at 568nm (red). The scale bar is 200 micrometers.
B: Scatter plot of average TBR2:BB intensity ratio in the ventricular-like zone/subventricular-like zone in "healthy" cortical organoids and "PRE" cortical organoids.
C: Scatter plot of average TBR2:BB intensity ratio in the cortical plate-like area in "healthy" cortical organoids and "PRE" cortical organoids.

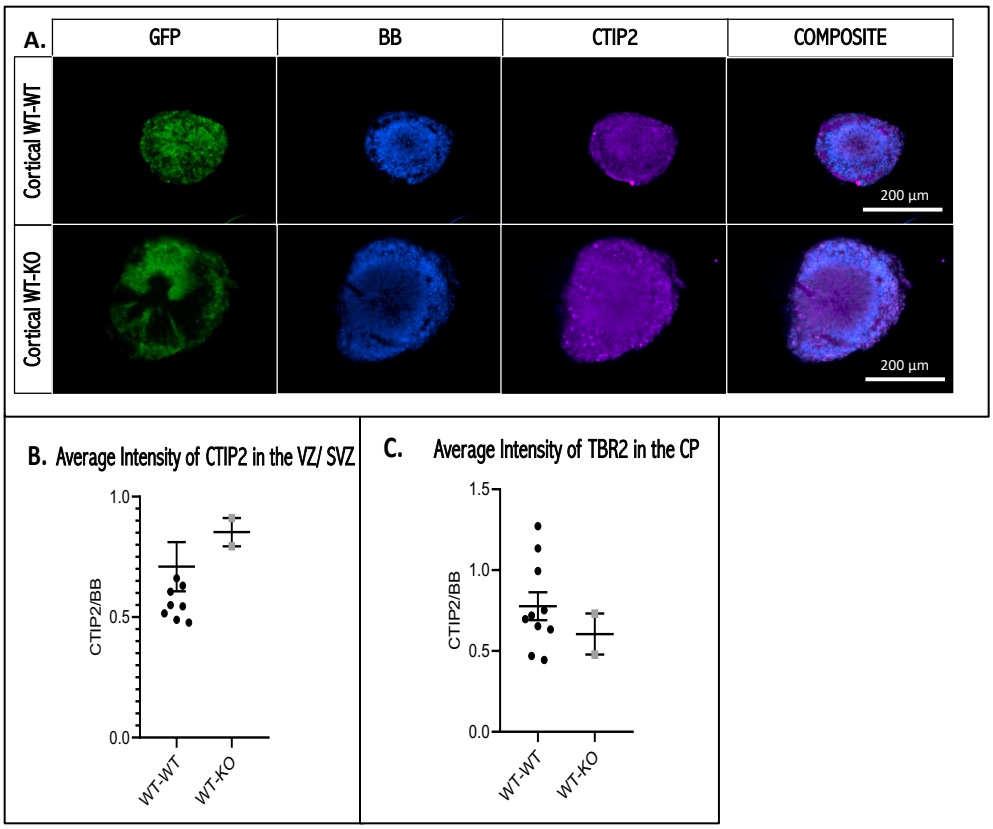

Figure 8: Immunocytochemistry and Quantification of CTIP2 in Cortical Organoids at Day 21.
A: Images of GFP, BB, and CTIP2 in "healthy" cortical organoids and "PRE" cortical organoids at Day 21. BB stains nuclei; CTIP2 is a deep laminal neuronal makrer in the cortical plate. BB and CTIP2 composite image shows the relative CTIP2 expression in "healthy" cortical organoids and "PRE" cortical organoids. GFP was imaged at 488nm (green), BB was imaged at 405nm (blue) and CTIP2 was imaged at 647nm (magenta). The scale bar is 200 micrometers.
B: Scatter plot of average CTIP2:BB intensity ratio in the ventricular-like zone/subventricular-like zone in "healthy" cortical organoids and "PRE" cortical organoids.
C: Scatter plot of average CTIP2:BB intensity ratio in the cortical plate-like area in "healthy" cortical organoids and "PRE" cortical organoids.

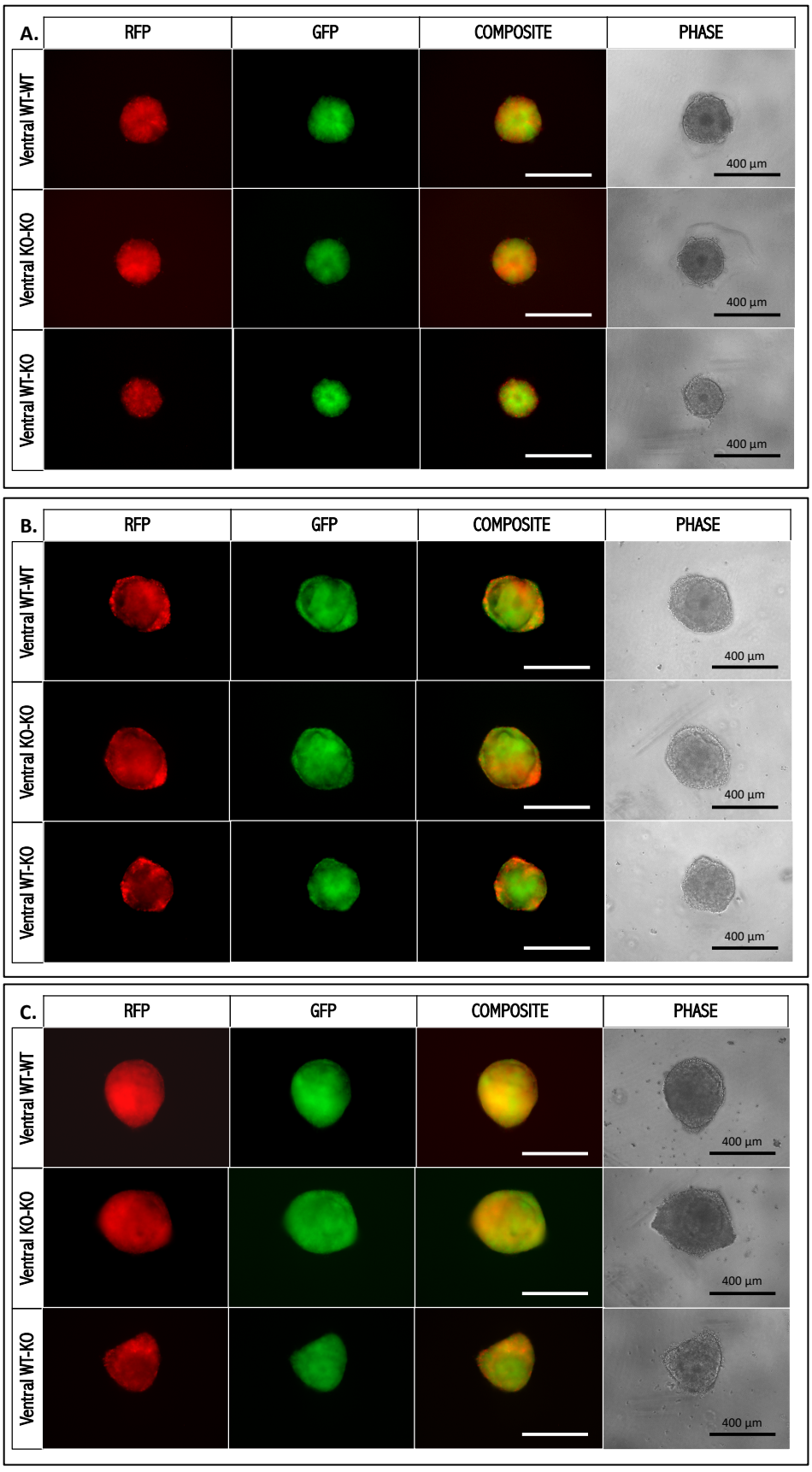

Figure 9: Live Imaging of RFP and GFP in Ventral Organoids at Days 13, 18, and 24. Images of RFP and GFP in "healthy" ventral organoids, "carrier" ventral organoids, and "PRE" ventral organoids at Days 13, 15, 20, and 34. RFP was imaged at 594nm (red) and GFP was imaged at 488nm (green). Phase image shows the structure of "healthy" ventral organoids, "carrier" ventral organoids, and "PRE" ventral organoids. The scale bar is 400 micrometers.
A: Images of RFP and GFP in "healthy" ventral organoids, "carrier" ventral organoids, and "PRE" ventral organoids at Day 13.
B: Images of RFP and GFP in "healthy" ventral organoids, "carrier" ventral organoids, and "PRE" ventral organoids at Day 18.
C: Images of RFP and GFP in "healthy" ventral organoids, "carrier" ventral organoids, and "PRE" ventral organoids at Day 24.

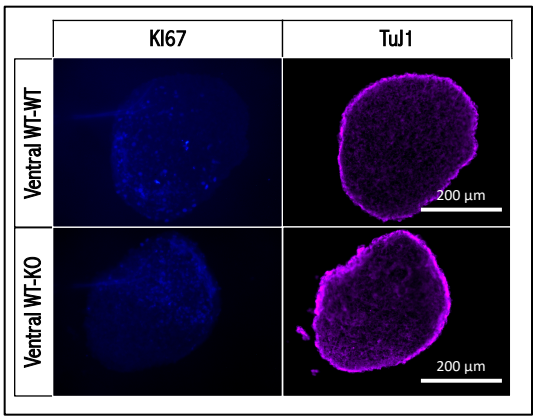

Figure 10: Immunocytochemistry of KI67 and TuJ1 in Ventral Organoids at Day 34.
Images of KI67 and TuJ1 in "healthy" ventral organoids and "PRE" ventral organoids at Day 34. KI67 is a proliferative cell marker; TuJ1 is a neuronal marker. KI67 was imaged at 405nm (blue) and TUJ1 was imaged at 647nm (magenta). The scale bar is 200 micrometers.